Diagnostic imaging of breast cancer using fluorescence-enhanced optical tomography: phantom studies

A. Godavarty
A. B. Thompson
R. Roy
M. Gurfinkel
Texas A&M University
Photon Migration Laboratory
College Station, Texas 77843-3573

M. J. Eppstein
C. Zhang
University of Vermont
Department of Computer Science
Burlington, Vermont 05405

E. M. Sevick-Muraca
Texas A&M University
Photon Migration Laboratory
College Station, Texas 77843-3573
E-mail: eva-m-sevick@tamu.edu

Abstract. Molecular targeting with exogenous near-infrared excitable fluorescent agents using time-dependent imaging techniques may enable diagnostic imaging of breast cancer and prognostic imaging of sentinel lymph nodes within the breast. However, prior to the administration of unproven contrast agents, phantom studies on clinically relevant volumes are essential to assess the benefits of fluorescence-enhanced optical imaging in humans. Diagnostic 3-D fluorescence-enhanced optical tomography is demonstrated using 0.5 to 1 cm^3 single and multiple targets differentiated from their surroundings by indocyanine green (micromolar) in a breast-shaped phantom (10-cm diameter). Fluorescence measurements of referenced ac intensity and phase shift were acquired in response to point illumination measurement geometry using a homodyned intensified charge-coupled device system modulated at 100 MHz. Bayesian reconstructions show artifact-free 3-D images (3857 unknowns) from 3-D boundary surface measurements (126 to 439). In a reflectance geometry appropriate for prognostic imaging of lymph node involvement, fluorescence measurements were likewise acquired from the surface of a semi-infinite phantom ($8 \times 8 \times 8$ cm^3) in response to area illumination (12 cm^2) by excitation light. Tomographic 3-D reconstructions (24,123 unknowns) were recovered from 2-D boundary surface measurements (3194) using the modified truncated Newton's method. These studies represent the first 3-D tomographic images from physiologically relevant geometries for breast imaging. © *2004 Society of Photo-Optical Instrumentation Engineers.* [DOI: 10.1117/1.1691027]

Keywords: optical tomography; fluorescence contrast agents; frequency-domain photon migration; breast cancer; molecular imaging; three-dimensional image reconstructions.

Paper 044008 received Jul. 7, 2003; revised manuscript received Dec. 10, 2003; accepted for publication Dec. 19, 2003.

1 Introduction

Imaging plays a central role in cancer diagnosis, therapy, and prognosis primarily through the detection of anatomically defined abnormalities, including calcifications that are often present in later-stage breast cancer. With the wealth of information provided by the now-maturing areas of genomics and proteomics, the identification of molecular markers and targets promises contrast-enhanced, diagnostic cancer imaging with a sensitivity and specificity to early cancer that is not possible with conventional, anatomical imaging. Molecular approaches promise to improve diagnostic cancer imaging and ultimately to affect the quality of cancer patient care.

While molecular imaging with exogenous agents may be universally attractive for most conventional imaging modalities such as magnetic resonance imaging (MRI), nuclear imaging [such as gamma imaging, positron emission tomography (PET), and single-photon emission computed tomography (SPECT)], and x-ray computed tomography (CT), molecular imaging requires sufficient signal arising from *minute* quanti-

ties of targeting agent. Magnetic resonance (MR) and x-ray imaging techniques typically require millimolar amounts of an exogeneous contrast agent, but recent advances in MRI have demonstrated that potential contrast can exist at concentrations as low as micromolar amounts. However, the amounts of exogeneous contrast agent required in MR and x-ray imaging are still substantial for sufficient signals for human imaging. Hence, the challenge of molecular diagnostic imaging of metastatic cancer typically lies with nuclear and optical techniques, which enable imaging using exogenous contrast agents at levels that are orders of magnitude smaller (<nanomolar).

Over the past 15 years, near-infrared (NIR) optical imaging approaches have been developed for breast cancer screening that are based upon an endogenous absorption contrast resulting from the nonspecific process of angiogenesis in order to discriminate normal from diseased tissues.[1–7] However, for diagnostic detection of early metastatic lesions in which the angiogenesis-induced contrast is nonexistent or insuffi-

cient for tomographic NIR imaging of the breast, exogenous contrast based upon targeting and reporting fluorophores will be necessary.[8–11] In the Photon Migration Laboratory at Texas A&M University, we have sought to develop fluorescence-enhanced optical tomography for breast cancer diagnosis via molecular imaging techniques. The approach depends upon delivering molecularly targeting NIR-excitable fluorescent contrast agents, which specifically target metastatic cancer cells within the breast tissue or, for prognostic indication of the extent of disease, within the lymph system draining the breast. Detection of cancer cells within the subsurface axillary lymph nodes, the internal mammary lymph nodes located beneath the medial sternum, or within the sentinel lymph node (or the lymph node closest to the primary breast tumor), which can be as great as 4 cm deep, is typically performed via biopsy following surgical resection. In the case of sentinel lymph nodes, it is performed following anatomical mapping using nuclear imaging and detection techniques, and prior to surgical resection and pathology.

However, before clinical feasibility trials involving the administration of a fluorescence contrast agent for diagnostic and prognostic imaging can begin, the efficacy of tomographic fluorescence-enhanced optical imaging in clinically relevant volumes must be demonstrated in phantom studies. To date, three-dimensional fluorescence-enhanced optical tomography has been limited to *in vivo* measurements in small animal models[12,13] or phantoms with unrealistic volumes or geometries[14–16] in comparison to what would be expected clinically.

In this paper, we present experimental tomographic imaging results involving two distinct measurement geometries pertinent to diagnostic and prognostic imaging of the breast within clinically relevant volumes and measured using an intensified charge-coupled device camera (ICCD) modified for time-dependent measurements of light propagation and fluorescence generation. In Sec. 2 we outline the necessity for the differing measurement geometries with point illumination and collection and area illumination and collection, and describe the light propagation model for fluorescence-enhanced optical imaging. The clinically relevant phantoms employed, the unique instrumentation involved in both measurement geometries, and a brief description of tomographic algorithms are given in Sec. 3. The experimentally obtained images that demonstrate the feasibility for state-of-the-art 3-D fluorescence-enhanced optical tomographic reconstructions on clinically relevant tissue phantoms are presented for the point and area illumination and collection geometries. Finally, these 3-D image reconstructions are discussed in light of the current ongoing clinical feasibility studies of fluorescence-enhanced optical imaging for mapping sentinel lymph nodes in breast cancer patients.

2 Background

The time-dependent technique for measuring light propagation and fluorescence generation used here involves the frequency-domain approach. In this approach, intensity-modulated, incident excitation light is delivered at a single point, at a series of points, or across an area on the tissue boundary, typically at modulation frequencies of 30 to 200 MHz. The excitation light or "photon density wave" propa-
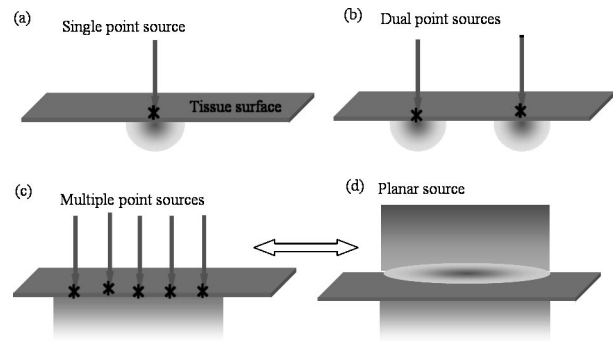

Fig. 1 Different measurement geometries. (a) Sequential point illumination of single excitation source using optical fibers. (b) Simultaneous point illumination of two excitation sources using optical fibers. (c) Simultaneous point illumination of multiple excitation sources using optical fibers. (d) Area illumination using an expanded beam of the excitation source. (c) and (d) are equivalent below the tissue surface, if the density of multiple-point illuminating sources is high.

gates as a spherical wave (in the case of point illumination) or a planar wave (in the case of area illumination). Owing to the absorption and scattering properties of the tissue, the excitation wave is amplitude attenuated and phase shifted relative to the incident wave. Upon encountering fluorescently tagged volumes within the tissue, a fluorescent photon density wave is generated with additional amplitude attenuation and phase lag, owing to the fluorescence decay kinetics of the fluorophore. This fluorescent photon density wave then propagates throughout the tissue, and during transit it experiences additional amplitude attenuation and phase lag owing to the tissue's optical properties until it reaches the tissue boundaries where it can be collected separately from the propagated excitation wave by optical filters.

Typically, all tomographic NIR imaging approaches (whether based upon endogenous or exogenous contrast) involve inverting measurements of light propagation between source–detector pairs of single, sequential points of excitation illumination and excitation (or emission) collection. Yet as shown in Fig. 1, illumination by excitation light from a single point interrogates a relatively small portion of tissue volume. Consequently, measurements among a series of single pairs of illumination and collection points must be accomplished using either spatial scanning or replication of the transmitters and receivers across the surface of the tissue. While these measurements are sufficient for the inverse spectroscopy problem, a limited set of point illumination and collection sites may produce sparse datasets for 3-D image reconstructions, especially when the fluorophore accumulates in an area not interrogated by the excitation light (Fig. 1). As a result, a high density of measurements in a relatively confined volume is typically required for imaging purposes, and simultaneous point illumination and area illumination and collection schemes in reflectance and\or transillumination geometries may be more appropriate.

Yet to date, while tomographic imaging algorithms have been developed for single illumination and collection measurements, to our knowledge there have been no attempts to tomographically reconstruct images from NIR measurements involving simultaneous point illumination and collection ge-

ometries or involving area illumination and collection geometries. In this work, we have extended tomographic imaging to include dual points of simultaneous illumination, as well as area illumination in order to enable interrogation of a larger tissue volume, as is appropriate for clinically relevant tissue volumes. Both simultaneous multiple-point sources and area illumination are being explored as means of (1) increasing the spatial coverage and the amount of NIR source light that can be safely delivered, and (2) decreasing the data acquisition time. Conceptually, as the number of point sources increases, the multiple-point illumination geometry [Fig. 1(c)] will mimic the area illumination geometry [Fig. 1(d)]. However in practice, the instruments for these two illumination geometries offer different opportunities and challenges since in one case optical fibers must contact the surface of the domain, and in the other case no optical fibers are involved. The general mathematical formulation of the light propagation model for both geometries is briefly presented in Sec. 2.1.

2.1 Diffusion Equation Model for Light Propagation in Tissue Medium Using Different Measurement Geometries

Measurements of diffusely propagated fluorescence are predicted by numerical solutions of the diffusion equation of light, given the true interior optical property map. The inverse imaging problem consists of using the forward solution of the diffusion equation in order to iteratively determine the interior optical property map, given the boundary measurements of diffusely propagated fluorescence. Owing to the enhanced sensitivity of time-resolved measurements to fluorescence over endogenous optical properties,[17,18] we employ finite-element (FE)-based numerical reconstruction algorithms in order to determine the interior optical property map of the absorption coefficient that is due to a fluorophore (μ_{axf}), which is directly related to the concentration of the fluorophore. The coupled diffusion equations for light propagation at a given modulation frequency, f ($\omega = 2\pi f$ radians) are given by[19–21]

$$-\nabla[D_x(\mathbf{r})\nabla\Phi_x(\mathbf{r},\omega)]+\left[\mu_{ax}(\mathbf{r})+\frac{i\omega}{c_x}\right]\Phi_x(\mathbf{r},\omega)=S$$
(1)

$$-\nabla[D_m(\mathbf{r})\nabla\Phi_m(\mathbf{r},\omega)]+\left(\mu_{am}(\mathbf{r})+\frac{i\omega}{c_m}\right)\Phi_m(\mathbf{r},\omega)$$

$$=\phi\mu_{a_{x\to m}}\frac{1}{1+i\omega\tau}\Phi_x(\mathbf{r},\omega),$$
(2)

where Φ_x and Φ_m are the ac components of the excitation and emission fluence (photons/s cm^2), and are given by $\Phi_{x,m} = I_{ACx,m}\exp(i\theta_{x,m})$. The term μ_{ax} is the sum of the absorption coefficients that are due to the chromophores (μ_{axi}, cm^{-1}) (i.e., the endogenous chromophores in tissues) and the fluorophores or the exogenous fluorescing agents (μ_{axf}, cm^{-1}); μ_{am} represents the sum of the absorption coefficients of the emission light that are due to the chromophores (μ_{ami}, cm^{-1}) and fluorophores (μ_{amf}, cm^{-1}); and ϕ and τ denote the quantum efficiency and lifetime (seconds) of the fluorophore, respectively. Also, c_x and c_m represent the velocity of

light at excitation and emission wavelengths (cm/s); ω corresponds to the modulation frequency of propagating light ($=2\pi f$ radians); and $\mathbf{r}$ is the positional vector. The optical diffusion coefficients, D_x and D_m for the excitation and emission light (centimeter) are given by

$$D_{x,m}=1/3[\mu_{ax,m}+\mu_{sx,m}(1-g)],$$
(3)

where g represents the anisotropy coefficient, which has a value >0.9 for biological tissues, and $\mu_{sx,m}$ are the scattering coefficients at excitation (suffix "x") and emission (suffix "m") wavelengths (cm^{-1}), respectively.

Representation of the source term in Eq. (1) depends upon the measurement geometry employed. A point illumination excitation source is represented as

$$S=\sum_{i=1}^{n} S\,\delta(\mathbf{r}-\mathbf{r}_s),$$
(4)

where $\mathbf{r}_s$ is the positional vector of the illuminating point, δ is the Dirac delta function representing the source of excitation light at a single point, and n is the total number of point illuminations ($n=1$ for single-point illumination and $n=2$ for simultaneous dual-point illumination). For the geometry of the area illuminated, the area of the planar source is discretized into a number of triangular finite elements and each elemental source is represented by

$$S=\sum_{i=1}^{3} L_i S_i,$$
(5)

where L_i consists of the x, y, z coordinates and S_i is the source value at each node (i) of the triangular element. Based on the type of elements used to discretize the phantom surface, the number of nodes (i) varies. If the discretization of the FE mesh is fine, then the source term corresponding to the area of illumination can be approximated as the summation of multiple point sources, given by Eq. (4), where n is the total number of nodes comprising the illuminated area.

Partial current boundary conditions were employed to solve the coupled diffusion equations and are given by[22]

$$\Phi_{x,m}(\mathbf{r},\omega)+2\gamma D_{x,m}(\mathbf{r})\frac{\partial\Phi_{x,m}(\mathbf{r},\omega)}{\partial n}=0,$$
(6)

where γ is the index-mismatch parameter and a function of the effective refractive index (R_{eff}) at the boundary surface, which is determined directly from Fresnel's reflections.[22,23]

The surface fluorescence measurements are used in image reconstruction algorithms along with the diffusion equation model in order to detect the target's location and size. In this work we employ the diffusion equation for recovery of the absorption coefficient that is due to the fluorophores (μ_{axf}) in two different phantom models that are appropriate for diagnostic and prognostic imaging of the breast. Details of the phantom models, the instrumentation, reconstruction algorithms, and the experimental design are discussed in Sec. 3.
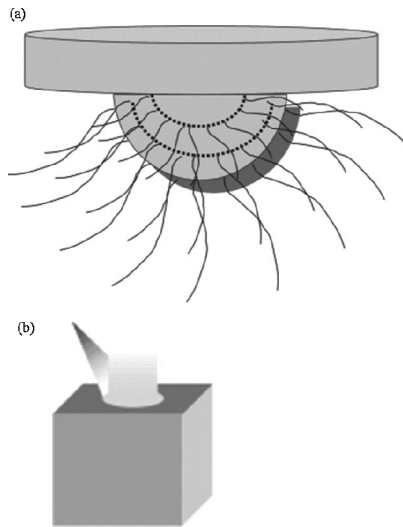
Fig. 2 Breast-shaped phantom with the cup-shaped portion (10-cm diameter) representing the breast tissue and the cylindrical portion (20-cm diameter and 2.5-cm height) representing the extended chest wall regions around the breast. Point illumination and collection measurement was employed on the hemispherical surface using optical fibers. (b) Semi-infinite phantom of $8 \times 8 \times 8$ cm^3 volume. Area illumination and detection was employed by illuminating and collecting a signal from a given area on the top surface of the phantom.

3 Materials and Methods

3.1 Phantoms

Parallel studies were performed using two different phantoms with differing measurement geometries. These include a breast-shaped phantom employing point illumination and collection geometry, and a semi-infinite phantom employing area illumination and collection geometry.

3.1.1 Breast-shaped phantom using point illumination and collection geometry

For tomographic evaluation of metastatic spread of cancer in the breast, we employed a breast-shaped phantom as shown in Fig. 2(a). The hemispherical portion of the phantom (10 cm diameter) was used to mimic the breast tissue and the extended chest wall regions around the breast (cylindrical portion, 20 cm diameter and 2.5 cm height). The measurement geometry for point illumination and collection was adapted to the breast phantom using optical fibers of 1-mm diameter that were located in concentric rings along the hemispherical surface of the phantom.[24] Most of the work performed in optical tomography employs a sequential point illumination and collection geometry, with recent developments toward imaging simultaneous multiple collection fibers using CCD cameras in continuous-wave (cw)[12,13] and frequency-domain photon migration (FDPM) approaches.[24–26] In our work, the collection of a light signal from the phantom surface was expedited by employing a CCD camera for simultaneous acquisition of data from multiple collection fibers that were interfaced as 2-D arrays onto an interfacing plate. Apart from a single-point illumination technique, a simultaneous dual in-phase point illumination technique [see Fig. 1(b)] was employed as a first step in evaluating the feasibility of tomographic reconstructions from measurements acquired using simultaneous

multiple-point illumination geometry [see Fig. 1(c)].[25] Fluorescence measurements were acquired from the entire hemispherical surface of the phantom; that is, 3-D boundary surface measurements were acquired for 3-D tomographic reconstructions.

3.1.2 Semi-infinite phantom using area illumination and collection geometry

For tomographic evaluation of the depth of a sentinel lymph node and for mapping lymph flow, current clinical feasibility trials involve area illumination of the upper quadrant of the breast, which is closest to the axilla, and area collection of the reemitted fluorescence signal. The phantom analogy to these clinical trials involves a semi-infinite model ($8 \times 8 \times 8$ cm^3 volume) [see Fig. 2(b)] employing area illumination and collection geometry. Here, the measurement geometry does not require any optical fibers to illuminate or collect the light signal. An expanded beam of modulated NIR light was incident on the top surface of the semi-infinite phantom and the emitted fluorescent signal was imaged directly using an intensified CCD camera detection system. Unlike point illumination of the excitation source, where the point source is not characterized, area illumination of the excitation source requires spatial characterization of the incident modulated NIR light. Hence, cross-polarizers are used to directly measure the excitation light specularly reflected (in terms of amplitude and phase) from the phantom's surface.[27,28]

As shown later, 3-D reconstructions were feasible with the semi-infinite phantom, even with 2-D boundary surface imaging from a single planar wave source. This measurement geometry mimics the prognostic imaging of a sentinel lymph node (from a 2-D boundary surface) in an actual clinical application.

3.2 Phantom Medium and Contrast Agents

Both phantoms were filled with a milky emulsion (1% Liposyn, Abbott Laboratories, North Chicago, Illinois) in order to mimic the highly scattering breast tissue. The optical properties of the background fluid were determined from FDPM measurements performed under infinite-medium conditions.[29]

Indocyanine green (ICG), a nonspecific blood pooling agent was employed as the fluorescing contrast agent, owing to its patient safety record in Food and Drug Administration-approved use for assessing hepatic function[30] and in retinal angiography.[31] ICG is most likely the best candidate for immediate clinical translation of the fluorescence-enhanced optical imaging technology, owing to its long-standing safety record in the clinic. When dissolved in water, ICG tends to exhibit excitation and emission maxima at 785 and 830 nm, with a quantum efficiency of 0.016 and a fluorescence lifetime of 0.56 ns.[17] The absorption coefficient that is due to the fluorescing contrast agent at both wavelengths ($\mu_{ax,m}$) was calculated using the following formula:

$$\mu_{ax,m} = 2.3\varepsilon_{ax,m}C, \tag{7}$$

where ε_{ax} is the extinction coefficient at the excitation wavelength (130,000 M^{-1} cm^{-1}), and ε_{am} is the extinction coefficient at the emission wavelength (22,000 M^{-1} cm^{-1}), and C is the concentration of ICG (microliters).
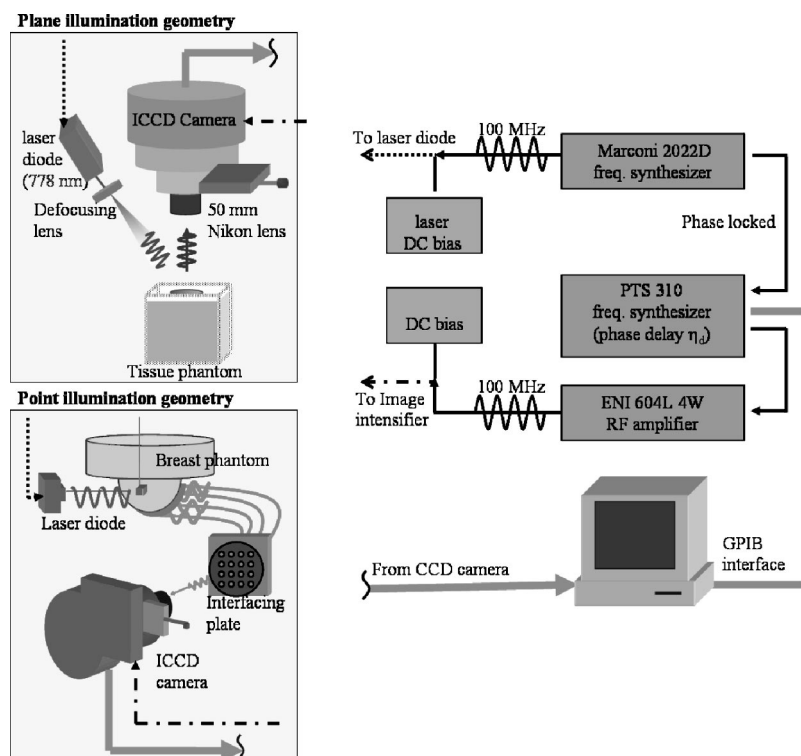
Fig. 3 Instrumentation for fluorescence-enhanced optical imaging in the frequency domain, using the gain-modulated intensified CCD camera for detection. The instrumentation setup is similar for both phantom systems, except for the measurement geometry employed in either phantom.

3.3 Instrumentation

Time-dependent fluorescent measurements were acquired in the frequency domain using a gain-modulated intensified CCD imaging system. A schematic of the instrumentation, along with the different measurement schemes employed in two different phantom experiments, is provided in Fig. 3. Modulated NIR light (783- or 785-nm wavelength) at 100 MHz was launched onto the phantom surface either through optical fibers or an expanded beam. In the breast phantom, dual excitation sources for a simultaneous dual-point illumination geometry were also obtained by splitting the laser source using a 50:50 beamsplitter (20Q20BS.2, Newport Corp., California). The modulating fluorescence signal emitted from both phantoms was acquired via a Nikon lens by the photocathode of the image intensifier (FS9910C Gen III model, IIT Night Vision, Roanoke, Virginia), which was also modulated at 100 MHz.

For measurement on the breast phantom using single- and dual-point illumination and multiple-point collection, the fluorescent signal collected by the fibers, whose ends were coupled to an interfacing plate, was acquired by the photocathode of the image intensifier. In contrast, fluorescence emitted from the boundary surface of the semi-infinite phantom was directly imaged onto the photocathode of the image intensifier. The fluorescent photons are converted to electrons at the photocathode, amplified at the multichannel plate, and converted back to photons at the phosphor screen of the image intensifier. These photons are in turn imaged by the CCD camera, which was either lens coupled (in the semi-infinite phantom system) or optically coupled (in the breast phantom system) to the phosphor screen of the image intensifier. A

16-bit CCD camera (Series AT200, model S1512B, Photometrics Ltd., Tucson, Arizona) was used for the semi-infinite phantom studies and a 12-bit CCD camera (TE/CCD-512-EFT Photometric CH12, Roper Scientific, New Jersey) was used for the breast phantom studies. The use of an ICCD detection system enhanced the data acquisition rates for both the phantoms, relative to the use of single-photon multiplier tubes (PMTs) for sequential detection, as employed in our earlier imaging studies.[14–16]

Measurements on both the phantoms were performed using the homodyne technique, since the laser diode and the photocathode of the image intensifier were modulated at the same frequency (100 MHz) using two oscillators that were phase locked by a 10-MHz reference signal. A phase delay varying from 0 to 2π was introduced between the two oscillators in order to obtain phase-sensitive constant-intensity images.[32] The ac intensity and phase shift were determined from the fast Fourier transform (FFT) that was performed on the 32 steady-state images acquired by varying the phase delay between the two oscillators. The data acquisition time varied with the integration time of the CCD camera (0.2 to 1 s), the number of phase delays acquired (32 in our case), and the total number of repetitions of each steady-state image (5 to 10). Further details regarding instrumentation and data acquisition procedures for both phantoms are described elsewhere.[24,27,32,33]

The weak fluorescent signal was collected by blocking the excitation light at the phantom surface using a stack of optical filters, including an 830-nm interference filter (F10-830.0-4-2.0 model, CVI Laser Corp., Albuquerque, New Mexico) and a holographic filter (HNPF-785.0-2.0 model, Kaiser Optical Systems Inc., Ann Arbor, Michigan). However, the filters

Table 1 Experimental conditions using different phantoms and illumination geometries.

Expt.	Phantom	Illumination geometry	Target to background ratio	[ICG] in target (μM)	Volume of target (cm^3)	No. of targets	Target depth (cm)
1	Breast	Single point	1:0	1.0	1	1	1.4
2	Breast	Dual point	1:0	1.0	1	1	1.4
3	Semi-infinite	Area	100:1	1.0	1	1	1
4	Breast	Single point	1:0	2.5	0.5 to 0.6	3	1.2 to 1.4

were not very efficient in completely rejecting the 785-nm excitation light, limiting the detection of deeply embedded targets in large phantom volumes regardless of the measurement geometries.[11,25] Work is currently underway to customize optical filters that can efficiently reject the excitation light without further attenuating the weak reemitted fluorescent signal.

For all experimental conditions, the acquired fluorescence measurements in terms of ac intensity (I_{ac}) and phase shift (θ) were referenced with respect to the measurement location having the maximum fluorescence ac intensity, in order to account for instrument response functions that affect the transmission of fluorescent signal from the phantom surface to the CCD detector array.[24,28]

3.4 Tomographic Reconstruction Algorithms

The coupled diffusion equations were solved for the fluence at excitation and emission wavelengths using a Galerkin finite-element approximation with tetrahedral elements.[34–37] Three-dimensional tomographic image reconstructions or solutions to the inverse imaging problem were obtained for both phantom studies using two different inversion approaches. In both inverse approaches, the surface-referenced fluorescence measurements of ac intensity and phase shift (represented as fluence in the diffusion model) were used along with the coupled diffusion equations in order to determine the 3-D interior optical property distribution of the unknown parameter, which was taken to be the absorption coefficient that is due to the fluorophores (μ_{axf}).

3.4.1 Approximate extended Kalman filter (AEKF) approach for breast phantom studies

In the case of breast phantom studies employing point illumination and collection, a Bayesian approach was used to reconstruct 3-D images of μ_{axf} using an approximate extended Kalman filter (AEKF) algorithm. In short, the AEKF is a minimum-variance approach in which the measurement error covariance and the dynamically estimated parameter error covariance are utilized in the regularization of the ill-posed inverse problem. Details of the algorithm are beyond the scope of this paper, but have been presented elsewhere.[16,24]

3.4.2 Penalty-modified barrier approach for semi-infinite phantom studies

In the case of semi-infinite phantom studies involving area illumination and collection, a constrained truncated Newton's (CONTN) method was employed.[38,39] The rate of convergence during the iterative image reconstruction scheme and the accuracy of the reconstructions were improved by incorporating a modified penalty/barrier method developed by Polyak[40] for constrained optimization problems. The modified barrier method has been shown to have a finite convergence as opposed to an asymptotic one, providing expeditious recovery of parameter maps. Details of this reconstruction algorithm are beyond the scope of this paper, but are presented elsewhere.[38–41]

3.5 Experimental Design

3.5.1 Experiments using a phantom model of the breast

Experiments were performed under varying experimental conditions of target to background optical contrast ratio (1:0, 100:1), different target depths (1 to 3 cm deep from the phantom surface to the centroid of the target), and different target volumes (0.5 and 1 cm^3) using micromolar concentrations of ICG as the fluorescing contrast agent. Fluorescence measurements were also acquired using single-point illumination geometry as well simultaneous dual-point illumination geometry in order to reconstruct 3-D images.

Here we present an example of a single target of 1-cm^3 volume located 1.4 cm deep under perfect uptake conditions of ICG, where both the single-point and dual-point illumination geometries were employed (see Table 1 for details). The current study was performed to demonstrate the feasibility of employing dual-point illumination geometry along with the widely employed single-point illumination geometry in order to tomographically reconstruct the target's location.[25] Another example is presented to mimic the diagnostic imaging of the multifocality of lesions in actual breast tissue. The study involved three small-volume targets (0.5 to 0.6 cm^3) located between 1.2 and 1.4 cm from the hemispherical surface of the phantom and under perfect uptake optical contrast conditions.

Table 2 Number of measurements and unknowns for image reconstructions in each experimental condition.

Expt.	Phantom	Illumination geometry	No. of measurements	No. of unknowns
1	Breast	Single point	126	3857
2	Breast	Dual point	439	3857
3	Semi-infinite	Area	3194	24,123
4	Breast	Single point	286	3857
4	Breast	Single point	286	11,906

Owing to the preliminary nature of the work, fluorescence measurements were acquired using only single-point and not dual-point illumination geometry.[26]

3.5.2 *Experiments using a semi-infinite phantom model*

Experiments were performed under varying target to background optical contrast ratios (1:0, 100:1) and target depths (1 to 2 cm deep from the imaging surface to the closest surface of the target) using a 1-cm^3 target volume and ICG as the fluorescing contrast agent. From a number of experimental studies,[28] only a single case is presented here as an example (experiment 3 in Table 1), in order to demonstrate the feasibility of reconstructing 3-D targets using 2-D reflectance measurements obtained from a single surface of a semi-infinite phantom. The total number of fluorescence measurements used during image reconstructions and the total number of unknowns in each discretized phantom are provided in Table 2 for all the experimental cases presented here.
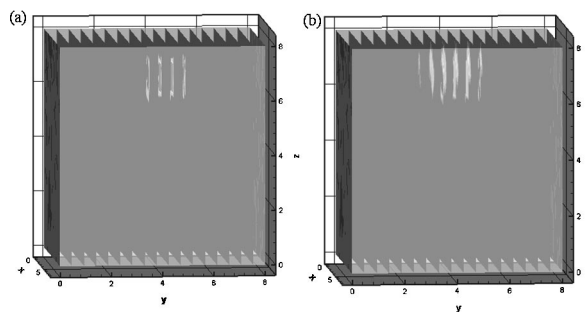

Fig. 5 (a) A series of contour slices along the y-plane of an actual cubic phantom, representing the true location of the 1-cm^3 target 1 cm from the top surface. (b) A series of contour slices along the y-plane of the reconstructed phantom, representing the reconstructed location of the target.

4 Results

The fluorescence measurements acquired from all experimental studies matched the simulated measurements predicted by the forward model reasonably well. Three-dimensional image reconstructions were made using the respective inversion approaches for the two phantoms; that is, a Bayesian approach for breast phantom studies and a modified truncated Newton's approach for the semi-infinite phantom studies.

Reconstructions obtained from the breast phantom experiments containing a single 1-cm^3 volume target located 1.4 cm deep with single- and dual-point illumination geometries are presented as a series of contour slices in the y-plane in Fig. 4.[25] Similar contour-sliced plots of the reconstructed semi-infinite phantom are presented in which a single 1-cm^3 volume target was located 1.4 cm deep from the boundary surface (see Fig. 5).[41] In both the phantoms and for all three different experimental cases, the single target was successfully
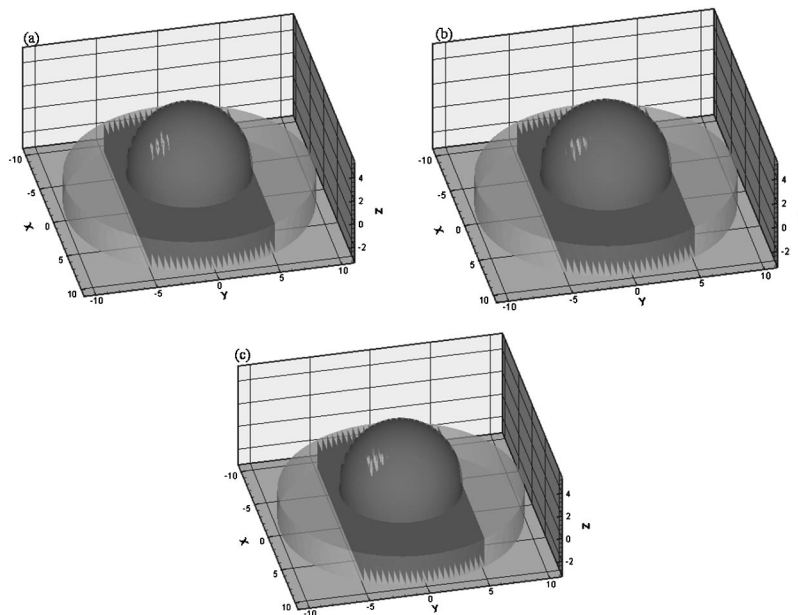

Fig. 4 (a) A series of contour slices along the y-plane of an actual breast phantom, representing the true location of the 1.4-cm^3 target located 1 cm from the hemispherical phantom surface. (b) A series of contour slices along the y-plane of the reconstructed breast phantom using single-point illumination. (c) Contour slices along the y-plane of the reconstructed breast phantom using simultaneous dual-point illumination.
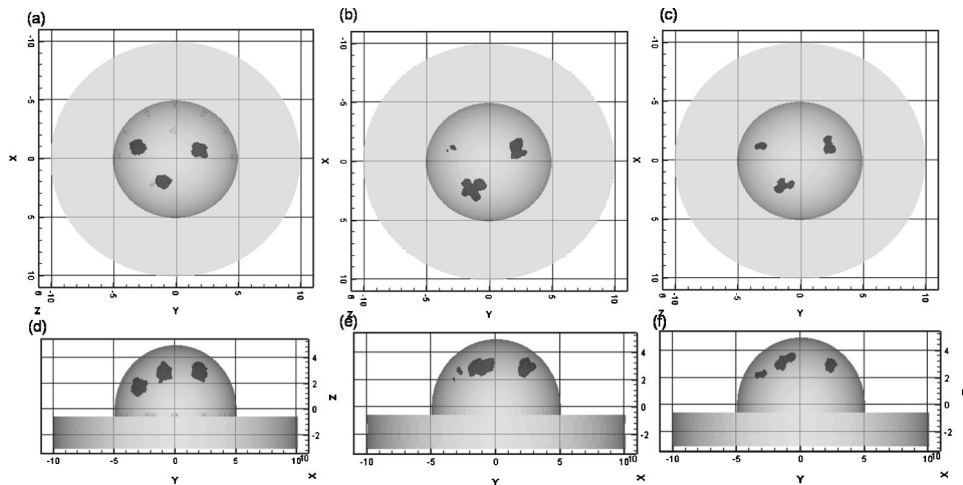
Fig. 6 (a) y-x and (d) y-z planar views of the actual breast phantom. (b) and (e) Reconstructed breast phantom using coarsely discretized mesh. (c) and (f) Reconstructed breast phantom using a finely discretized mesh. Three targets of 0.5 to 0.6 cm^3 volume were used in the actual breast phantom of $\sim$1087 cm^3 volume and measured using single-point illumination geometry.

reconstructed close to its true location without any spatial artifacts. Single, 1-cm^3 volume targets located 2 cm deep were also reconstructed in the breast phantom.[25] For brevity and for comparison with the reconstructions from the area illumination and collection measurements, only the results from the 1-cm deep target are presented here.

Image reconstructions were also performed for the breast phantom experiment containing three small-volume targets (0.5 to 0.5 cm^3) located up to 1.4 cm deep from the phantom surface (experiment 4 of Table 1). The initial reconstructions used a discretized mesh phantom (3857 unknowns) similar to that used for the single 1-cm^3 volume target studies. Using this coarsely discretized mesh phantom, one of the three targets was not completely located and appeared as an artifact [see Figs. 6(b) and 6(e)], even though the reconstructions converged. Upon employing a more finely discretized breast phantom (11,906 unknowns) under similar reconstruction conditions, all three targets were distinctly located without any artifacts [see Figs. 6(c) and 6(f)].[26] This result could probably be attributed to the level of FE mesh discretization, in which the distance between two consecutive nodes in the mesh, if equivalent to the radius of the target, could reduce the probability of reconstructing the target. It should be noted that these breast phantom studies, which attempt to mimic the multifocality of lesions within the breast, are preliminary and more work is under way to assess the significance of discretization for detecting the smallest possible target volumes.

5 Discussion

Future diagnostic and prognostic breast imaging with NIR must be directed toward molecular targeting of single and multiple lesions. To realize these goals, simultaneous development of (1) fluorescence-enhanced optical imaging systems using clinically relevant phantom systems and different possible measurement geometries, and (2) reconstruction algorithms to solve for the highly ill-posed inversion problem, where sparse surface measurements are used to determine the 3-D interior optical property maps, must be undertaken. Only a few examples of such reconstructions are presented here, in order to demonstrate for the first time the feasibility of tomographically reconstructing large 3-D phantoms of clinical relevance, and using different measurement geometries. Work is progressing toward assessment of their robustness using different measurement geometries and under varying experimental conditions, in order to aid in the clinical translation of the emerging fluorescence-enhanced optical imaging technology.

Breast phantom studies using point illumination and collection geometry have the potential for a direct translation into clinical diagnostic imaging of breast tissue by molecularly targeting the metastatic spread of lesions or early-stage lesions using a systemic, intravenously injected fluorescent contrast agent. The feasibility of employing dual-point illumination measurement geometry in breast phantoms can be easily translated into simultaneous multiple-point illumination geometry for clinical feasibility trials, prior to which the sensitivity and specificity of this imaging modality must be assessed using different phantom models.

The preliminary semi-infinite phantom studies using area illumination and collection geometry have demonstrated the possibility of prognostic imaging of sentinel lymph nodes and of locating nodes for surgical resection. Although initial clinical feasibility trials are using a nonspecific contrast agent (ICG), parallel feasibility studies are currently being performed to develop and assess the performance of tumor-specific contrast agents through small-animal studies.[42]

Future development critically depends upon improving rejection of excitation light, enabling tomographic reconstructions of smaller targets at greater depths and with lower concentrations (up to nanomolar amounts) of the fluorophores. The ability to collect a signal from 100 fmol of ICG at tissue depths of 4 cm and greater[11] needs to be effectively transferred to clinical breast imaging.

References

1. M. A. Franceschini, K. T. Moesta, S. Fantini, G. Gaida, E. Gratton, H. Jess, W. W. Mantulin, M. Seeber, P. M. Schlag, and M. Kaschke, "Frequency-domain techniques enhance optical mammography: initial clinical results," *Proc. Natl. Acad. Sci. U.S.A.* **94**, 6468–6473 (1997).

2. S. Fantini, S. A. Walker, M. A. Franceschini, M. Kaschke, P. M. Schlag, and K. T. Moesta, "Assessment of the size, position, and optical properties of breast tumors *in vivo* by noninvasive optical methods," *Appl. Opt.* **37**(10), 1982–1989 (1998).

3. K. T. Moesta, S. Fantini, H. Jess, S. Totkas, M. A. Franceschini, M. Kaschke, and P. M. Schlag, "Contrast features of breast cancer in frequency-domain laser scanning mammography," *J. Biomed. Opt.* **3**(2), 129–136 (1998).

4. D. Grosenick, H. Wabnitz, H. H. Rinneberg, K. T. Moesta, and P. M. Schlag, "Development of a time-domain optical mammograph and first *in vivo* applications," *Appl. Opt.* **38**(13), 2927–2943 (1999).

5. S. B. Colak, M. B. van der Mark, G. W. 't Hooft, J. H. Hoogenraad, E. S. van der Linden, and F. A. Kuijpers, "Clinical optical tomography and NIR spectroscopy for breast cancer detection," *IEEE J. Sel. Top. Quantum Electron.* **5**(4), 1143–1158 (1999).

6. B. W. Pogue, S. P. Poplack, T. O. McBride, W. A. Wells, K. S. Osterman, U. L. Osterberg, and K. D. Paulsen, "Quantitative hemoglobin tomography with diffuse near-infrared spectroscopy: pilot results in the breast," *Radiology* **218**(1), 261–266 (2001).

7. H. Jiang, Y. Xu, N. Iftimia, J. Eggert, K. Klove, L. Baron, and L. Fajardo, "Three-dimensional optical tomographic imaging of breast in a human subject," *IEEE Trans. Med. Imaging* **20**(12), 1334–1340 (2001).

8. D. J. Hawrysz and E. M. Sevick-Muraca, "Developments toward diagnostic breast cancer imaging using near-infrared optical measurements and fluorescent contrast agents," *Neoplasia* **2**(5), 388–417 (2000).

9. K. Licha, "Contrast agents for optical imaging," *Top. Curr. Chem.* **222**, 1–29 (2002).

10. M. Gurfinkel, S. Ke, X. Wen, C. Li, and E. M. Sevick-Muraca, "Near-infrared fluorescence optical imaging and tomography," *Disease Markers* (in press) 2004.

11. J. P. Houston, A. B. Thompson, M. Gurfinkel, and E. M. Sevick-Muraca, "Sensitivity and depth penetration of continuous wave *versus* frequency-domain photon migration near-infrared fluorescence contrast-enhanced imaging," *Photochem. Photobiol.* **77**, 420–430 (2003).

12. V. Ntziachristos and R. Weissleder, "Experimental three-dimensional fluorescence reconstruction of diffuse media by use of a normalized Born approximation," *Opt. Lett.* **26**(12), 893–895 (2001).

13. V. Ntziachristos and R. Weissleder, "Charge-coupled-device based scanner for tomography of fluorescent near-infrared probes in turbid media," *Med. Phys.* **29**(5), 803–809 (2002).

14. D. J. Hawrysz, M. J. Eppstein, J. Lee, and E. M. Sevick-Muraca, "Error consideration in contrast-enhanced three-dimensional optical tomography," *Opt. Lett.* **26**(10), 704–706 (2001).

15. J. Lee and E. M. Sevick-Muraca, "3-D Fluorescence enhanced optical tomography using reference frequency-domain photon migration measurements at emission and excitation measurements," *J. Opt. Soc. Am. A* **19**(4), 759–771 (2002).

16. M. J. Eppstein, D. J. Hawrysz, A. Godavarty, and E. M. Sevick-Muraca, "Three-dimensional, near-infrared fluorescence tomography with Bayesian methodologies for image reconstruction from sparse and noisy data sets," *Proc. Natl. Acad. Sci. U.S.A.* **99**, 9619–9624 (2002).

17. E. M. Sevick-Muraca, G. Lopez, T. Troy, J. S. Reynolds, and C. L. Hutchinson, "Fluorescence and absorption contrast mechanisms for biomedical optical imaging using frequency-domain techniques," *Photochem. Photobiol.* **66**, 55–64 (1997).

18. M. J. Eppstein, D. E. Dougherty, D. J. Hawrysz, and E. M. Sevick-Muraca, "Three-dimensional Bayesian optical image reconstruction with domain decomposition," *IEEE Trans. Med. Imaging* **20**(3), 147–163 (2000).

19. E. M. Sevick and C. L. Burch, "Origin of phosphorescence signals reemitted from tissues," *Opt. Lett.* **19**(23), 1928–1930 (1994).

20. M. S. Patterson and B. W. Pogue, "Mathematical model for time-resolved and frequency-domain fluorescence spectroscopy in biological tissues," *Appl. Opt.* **33**, 1963–1974 (1994).

21. C. L. Hutchinson, J. R. Lakowicz, and E. M. Sevick-Muraca, "Fluorescence life-time based sensing in tissues: a computational study," *Biophys. J.* **68**, 1574–1582 (1995).

22. R. C. Haskell, L. O. Scasssand, T-T. Tsay, T-C. Feng, M. S. McAdams, and B. J. Tromberg, "Boundary conditions for the diffusion equation in radiative transfer," *J. Opt. Soc. Am. A* **11**, 2727–2741 (1994).

23. A. Godavarty, D. J. Hawrysz, R. Roy, E. M. Sevick-Muraca, and M. J. Eppstein, "Influence of the refractive index-mismatch at the boundaries measured in fluorescence-enhanced frequency-domain photon migration imaging," *Opt. Express* **10**(15), 653–662 (2002).

24. A. Godavarty, M. J. Eppstein, C. Zhang, S. Theru, A. B. Thompson, M. Gurfinkel, and E. M. Sevick-Muraca, "Fluorescence-enhanced optical imaging in large tissue volumes using a gain modulated ICCD camera," *Phys. Med. Biol.* **48**(21), 1701–1720 (2003).

25. A. Godavarty, C. Zhang, M. J. Eppstein, and E. M. Sevick-Muraca, "Fluorescence-enhanced optical imaging of large phantoms using single and simultaneous dual point illumination geometries," *Med. Phys.* **31**(2), 183–190 (2004).

26. A. Godavarty, M. J. Eppstein, C. Zhang, and E. M. Sevick-Muraca, "Detection of single and multiple targets in tissue phantoms using fluorescence-enhanced optical imaging: a feasibility study," Radiology (submitted) (2004).

27. A. B. Thompson and E. M. Sevick-Muraca, "Near-infrared fluorescence contrast-enhanced imaging with intensified charge-coupled device homodyne detection: measurement precision and accuracy," *J. Biomed. Opt.* **8**(1), 111–120 (2003).

28. A. Thompson, D. J. Hawrysz, and E. M. Sevick-Muraca, "Near-infrared fluorescence contrast-enhanced imaging with area illumination and area detection: the forward imaging problem," *Appl. Opt.* **42**(19), 4125–4136 (2003).

29. Z. Sun, Y. Huang, and E. M. Sevick-Muraca, "Precise analysis of frequency domain migration measurement for characterization of concentrated colloidal suspensions," *Rev. Sci. Instrum.* **73**(2), 383–393 (2002).

30. C. M. Leevy, F. Smith, and J. Longueville, "Indocyanine green clearance as a test for hepatic function: evaluation by dichromatic ear densitometry," *J. Am. Med. Assoc.* **200**, 236–240 (1967).

31. K. Kogure, N. J. David, U. Yamanouchi, and E. Choromokos, "Infrared absorption angiography of the fundus circulation," *Arch. Ophthalmol.* **83**(2), 209–214 (1970).

32. J. R. Lakowicz and K. W. Berndt, "Lifetime-selective fluorescence imaging using an rf phase-sensitive camera," *Rev. Sci. Instrum.* **62**(7), 1727–1734 (1991).

33. J. S. Reynolds, T. L. Troy, and E. M. Sevick-Muraca, "Multipixel techniques for frequency-domain photon migration imaging," *Biotechnol. Prog.* **13**(5), 669–680 (1997).

34. O. C. Zeinkiewicz and R. L. Taylor, *The Finite Element Methods in Engineering Science*, McGraw-Hill, New York (1989).

35. J. N. Reddy, *An Introduction to the Finite-Element Method*, 2nd ed., McGraw-Hill, New York (1993).

36. R. Roy and E. M. Sevick-Muraca, "Truncated Newton's optimization scheme for absorption and fluorescence optical tomography: Part I. Theory and formulation," *Opt. Express* **4**, 353–371 (1999).

37. F. Fedele, J. P. Laible, and M. J. Eppstein, "Coupled complex adjoint sensitivities for frequency-domain fluorescence tomography: theory and vectorized implementation," *J. Comput. Phys.* **187**, 597–619 (2003).

38. R. Roy, and E. M. Sevick-Muraca, "Active constrained truncated Newton method for simple-bound optical tomography," *J. Opt. Soc. Am. A* **17**, 1627–1641 (2000).

39. R. Roy and E. M. Sevick-Muraca, "Three-dimensional unconstrained and constrained image-reconstruction techniques applied to fluorescence, frequency-domain photon migration," *Appl. Opt.* **40**, 2206–2215 (2001).

40. R. Polyak, "Modified barrier functions (theory and methods)," *Math. Program.* **54**, 177–222 (1992).

41. R. Roy, A. B. Thompson, A. Godavarty, and E. M. Sevick-Muraca, "Tomographic fluorescence imaging in tissue phantoms: a novel reconstruction algorithm and imaging geometry," *IEEE Trans. Med. Imaging* (submitted) (2004).

42. S. Ke, X. Wen, M. Gurfinkel, C. Charnsangavej, S. Wallace, E. M. Sevick-Muraca, and C. Li, "Near-infrared optical imaging of epidermal growth factor receptor in breast cancer xenografts," *Cancer Res.* **63**, 7870–7875 (2003).